INTERNATIONAL JOURNAL OF NUMERICAL MODELLING: ELECTRONIC NETWORKS, DEVICES AND FIELDS
Int. J. Numer. Model. 0000; **00**:1–14

Analysis of cutoff wavelength of elliptical waveguide by regularized meshless method

Rencheng Song and Xudong Chen*

Department of Electrical and Computer Engineering, National University of Singapore, Singapore

SUMMARY

In this paper, the regularized meshless method (RMM) combined with the determinant rule is taken to analyze the cutoff wavelength of elliptical waveguide with arbitrary eccentricity. First, an improved desingularization technique of subtracting and adding-back is introduced for RMM to discretize this problem. Then the novel local minimum finding technique based on Chebfun is applied to extract the cutoff wavelength from the determinant of the interpolation matrix of RMM. The numerical examples show the RMM gets consistent results with the conventional method of fundamental solutions, but has advantage of well-conditioning and no fictitious boundary. Our method provides another highly effective and stable candidate to solve the cutoff wavelength of elliptical waveguide. Copyright © 0000 John Wiley & Sons, Ltd.

KEY WORDS: cutoff wavelength, elliptical waveguide, regularized meshless method, the method of fundamental solutions, Chebfun

1. INTRODUCTION

The elliptical waveguides have been studied for several decades and are widely used in various microwave components [1]. The calculation of the cutoff wavelength of elliptical waveguides is important for the waveguide design and wave propagation analysis. A large number of techniques have been presented and one of the first known paper was owed to Chu [2]. Most of these methods are based on the cumbersome roots finding for the modified Mathieu functions of the first kind. In recent years, some new methods have been proposed to simplify and improve the solution calculation of cutoff wavelength. We only list some recent progress about this issue. In [3], Mei and Xu calculated the cutoff wavelength of the dominant mode in elliptical waveguide by the transverse resonance technique. Tsogkas *et al.* [4] provided the exact closed-form algebraic expressions of cutoff wavelength for elliptical metallic waveguide with small values of eccentricity. In [5], Shu analyzed the elliptical waveguides with arbitrary ellipticity by the differential quadrature method (DQ), which combines with the coordinate transform to deal with the elliptical shape boundary. In

*Correspondence to: Department of Electrical and Computer Engineering, National University of Singapore, 117576 Singapore. Email: elesongr@nus.edu.sg (Song), and elechenx@nus.edu.sg (Chen).

Prepared using jnmauth.cls *[Version: 2010/03/27 v2.00]*

[6], Jiang *et al.* presented a meshless collocation method with the Wendland radial basis functions. Their method can deal with the elliptical domain directly.

Besides these methods, Young *et al.* [7] presented a simple and high-accuracy method based on the method of fundamental solutions (MFS) together with the singular value decomposition (SVD). Different from [5, 6], this method is a boundary type meshless method, which doesn't need to discretize the interior domain. Its basic idea is to discretize the cutoff wavelength problem by the MFS and form a matrix equation taking the unknown cutoff wavelength λ_c as parameter. Then the SVD is employed to determine λ_c. However, the MFS has two main drawbacks such as the fictitious boundary and ill-conditioned interpolation matrix. Its solution accuracy and stability depend seriously on the locations of source nodes. There are many remedial methods to overcome these two issues of MFS. The regularized meshless method (RMM) [10] is one of the best candidates. It takes the double layer potential as basis function and is also a boundary type meshless method. The RMM in [10] applies the desingularization technique of subtracting and adding-back so as to choose the source nodes coincident with the collocation nodes on the physical boundary. It has been successfully applied in various numerical studies [10, 11, 12, 13, 14], which show that the RMM keeps all merits of the MFS but overcome the disadvantages mentioned before. Particularly, the RMM has been used in [15] to solve the acoustic eigenproblem with multiply-connected domain. However, the conventional RMM is mostly used in regular domain problems due to the limitation of desingularization technique [16]. It requires the nodes distribute uniformly on the boundary, which is difficult or impossible to realize in irregular domains. We showed a modified desingularization technique in [16] such that the RMM can deal with arbitrary domain problems.

In this study, we will introduce a further improved desingularization technique for RMM such that it can solve the cutoff wavelength of elliptical waveguide and in addition remove the numerical integral calculation needed in [16]. Then the RMM is taken to discretize the cutoff wavelength problem and the determinant rule is chosen to figure out the cutoff wavelength. Since the cutoff wavelength λ_c corresponds to local minimum of the non-smooth determinant function, the generally used Newton method fails. Usually the time-consuming scanning method, i.e., plotting figure with very fine grid, is used to find the local minima. Besides the low efficiency, the scanning method may also miss the correct solution if its step is too large. In this paper, we will introduce a novel local minimum finding technique based on Chebfun [17]. To summarize, our paper has three contributions. Firstly, we introduce the RMM with improved desingularization technique to deal with elliptical boundary so as to overcome the disadvantage of the MFS in [7]. Secondly, the local minimum finding technique based on Chebfun is used to improve the efficiency and stability. Thirdly, numerical comparisons between our method and the MFS [7] will also be provided.

In this paper, only the TM mode is considered to illustrate our algorithm. The structure of this paper is as follows. Section 2 introduces the problem and reviews the MFS. Our proposed method is presented in Section 3. Numerical examples are shown in Section 4. Finally, conclusions are made in Section 5.

DOI: 10.1002/jnm

2. THE PROBLEM AND THE MFS METHOD

2.1. The problem

The cutoff wavelength of TM mode for two dimensional elliptical waveguide satisfies

$$\nabla^2\phi + \kappa_c^2\phi = 0, \tag{1}$$

where $\phi(x, y) = E_z(x, y)$, $k_c = 2\pi/\lambda_c$ is the cutoff wavenumber, and λ_c is the cutoff wavelength.

The TM wave satisfies the Dirichlet boundary condition (BC)

$$\phi|_\Gamma = E_z|_\Gamma = 0, \tag{2}$$

where Γ is the elliptical boundary satisfying

$$\left(\frac{x}{a}\right)^2 + \left(\frac{y}{b}\right)^2 = 1. \tag{3}$$

The parameters a and b are the semi-major and semi-minor axes respectively. So $e = \sqrt{a^2 - b^2}/a$ is the eccentricity. Our aim is to solve λ_c for elliptical waveguides with different eccentricities.

2.2. The MFS method

We briefly introduce the MFS in [7]. Let

$$\phi(t) = \sum_{j=1}^{N} \alpha_j G(t, s_j), \tag{4}$$

where $t = (x, y)$ is node in the solution domain, $\{s_j\}_{j=1}^N$ are source nodes, and $\{\alpha_j\}_{j=1}^N$ are unknown coefficients. The basis functions $\{G(t, s_j)\}_{j=1}^N$ of the MFS for 2-D Helmholtz equation are [8]

$$G(t, s_j) = -\frac{\mathbf{i}}{4} H_0^{(2)}(\kappa r(t, s_j)), \quad j = 1, 2, \ldots, N \text{ in } \mathbb{R}^2, \tag{5}$$

where $\mathbf{i} = \sqrt{-1}$, $H_0^{(2)}(\kappa r(t, s_j))$ is the zero order of second kind Hankel function, and $r(t, s_j) = \|s_j - t\|_2$. The basis functions in Equation (5) satisfy the Helmholtz equation. Thus, the MFS is a boundary-only meshless method.

As seen in Equation (5), there is a singularity in Hankel function when $r = 0$. Thus, the MFS selects the source nodes $\{s_j\}_{j=1}^N$ on a fictitious boundary outside the domain. For our problem, the source nodes of MFS are set on a larger ellipse with the same eccentricity as boundary Γ, see Figure 1. Suppose the fictitious ellipse has semi-major axis length $wa(w > 1)$.

Since the basis function satisfies the governing equation, the MFS only needs to match the BC at the M boundary nodes, namely,

$$\phi(t_i) = \sum_{j=1}^{N} \alpha_j G(t_i, s_j) = 0, \quad i = 1, 2, \ldots, M. \tag{6}$$

Prepared using jnmauth.cls
DOI: 10.1002/jnm

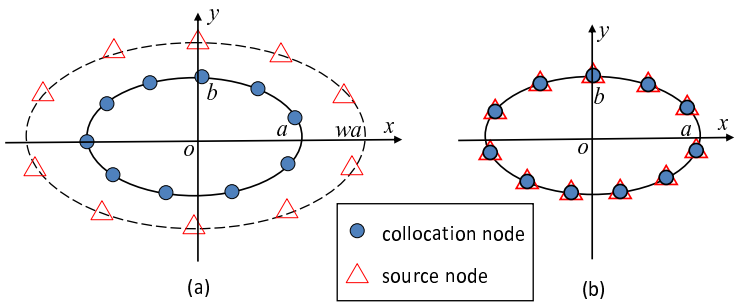

Figure 1. Nodes distribution. (a) MFS; (b) RMM.

For easy of comparing with RMM, we suppose $M = N$ hereafter. It means the same number of collocation and source nodes are used in MFS. By this collocation technique, we rewrite Equation (6) in matrix form as

$$B(\lambda)\boldsymbol{\alpha} = \mathbf{0}, \tag{7}$$

where $B(\lambda) = (G(t_i, s_j))_{N\times N}$ is the coefficient matrix with $\lambda = 2\pi/\kappa$ as parameter, and $\boldsymbol{\alpha}$ is the unknown coefficient vector.

As previously mentioned, theoretically, $B(\lambda)$ should be singular when $\lambda = \lambda_c$. According to this property, λ_c can be solved by searching the zeros of

$$f_1(\lambda) = \min(\mathrm{svd}(B(\lambda))) \tag{8}$$

or

$$f_2(\lambda) = |\det(B(\lambda))|, \tag{9}$$

where $\min(\mathrm{svd}(B(\lambda)))$ indicates the minimal singular value of $B(\lambda)$ and $|\det(B(\lambda))|$ is the absolute value of its determinant. In [7], the SVD function $f_1(\lambda)$ is applied, while we will take use of Equation (9) in our method. In practical computation, only finite number of basis functions are taken to approximate $\phi(t)$. Thus, the obtained interpolation matrix $B(\lambda)$ may be nonsingular even at the cutoff wavelength. In such case, the roots searching of $f_j(\lambda), j = 1, 2$ is numerically meaningless. Actually, if we take $G(t, s_j) = -c\frac{\mathbf{i}}{4}H_0^{(2)}(\kappa r(t, s_j))$ as the basis function for the MFS where c is a constant value. This doesn't change the solution of the MFS. However, the value of $f_2(\lambda) = |\det(cB(\lambda))| = c^N|\det(B(\lambda))|$ can be arbitrarily large if c is properly chosen. Thus, in our computation, the local minima of $f_2(\lambda)$ are solved instead of searching its roots, so as for the following RMM. If not specifically specified, f_2 is denoted as f hereafter.

DOI: 10.1002/jnm

3. THE REGULARIZED MESHLESS METHOD

3.1. The RMM

To solve the problem in Equations (1) and (2), the RMM takes the double layer potential functions as basis functions [10, 15]

$$T(t,s_j)=-\frac{\mathbf{i}\pi\kappa}{2}H_1^{(1)}(\kappa r(t,s_j))\frac{\langle (t-s_j),n_j\rangle}{r(t,s_j)},\quad j=1,2,\ldots,N \tag{10}$$

where $H_1^{(1)}(\cdot)$ is the first order of the first kind Hankel function, the sign $\langle\cdot,\cdot\rangle$ indicates the inner product of two vectors, and n_j is the outward normal direction at s_j. As seen, $T(t,s_j)$ satisfies the governing Helmholtz equation. So RMM is also a boundary-type meshless method.

Although the basis function in Equation (10) has singularity, a desingularization technique was introduced in [10] such that the source nodes can be coincident with the collocation nodes on the domain boundary, see Figure 1. We will briefly introduce this technique, point out its shortage, and then improve it.

As shown in [10], $T(t,s_j)$ has the same order singularity as the RMM basis function for Laplace equation [13, 15] when t approaches to s_j, namely,

$$\lim_{t\to s_j}T(t,s_j)=\lim_{t\to s_j}A(t,s_j), \tag{11}$$

where $A(t,s_j)=-\dfrac{\langle (t-s_j),n_j\rangle}{r(t,s_j)^2}$ is the double layer potential of Laplace equation [10].

The desingularization technique of subtracting and adding-back is based on the discretization of the reduced null-fields equation [9, 10]

$$\int_\Gamma A^{(e)}(t_i,s)d\Gamma(s)=0,\quad t_i\in D^e, \tag{12}$$

where $A^{(e)}$ has the opposite normal direction with A, and D^e is the exterior domain of $\overline{D}$. According to the relation of $A^{(e)}$ and A, there is [10]

$$\begin{cases} A(t_i,s_j)=-A^{(e)}(t_i,s_j), & i\neq j,\\ A(t_i,s_j)=A^{(e)}(t_i,s_j), & i=j. \end{cases} \tag{13}$$

In the RMM, Equation (12) is discretized as

$$\sum_{j=1}^{N}A^{(e)}(t_i,s_j)|l_j|=0,\quad t_i\in\Gamma, \tag{14}$$

where $|l_j|$ is the half distance between the source nodes s_{j-1} and s_{j+1}. Generally, the nodes $\{s_j\}_{j=1}^N$ are supposed to be uniform in RMM such that $\{|l_j|\}_{j=1}^N$ are equal for different j. Thus, Equation (14) can be reduced to

$$\sum_{j=1}^{N}A^{(e)}(t_i,s_j)=0,\quad t_i\in\Gamma. \tag{15}$$

DOI: 10.1002/jnm

By collocating on boundary nodes, we get

$$\begin{aligned}\phi(t_i) &= \sum_{j=1}^{N} \beta_j T(t_i, s_j) \\ &= \sum_{j=1}^{N} \beta_j T(t_i, s_j) - \beta_i \sum_{j=1}^{N} A^{(e)}(t_i, s_j) \\ &= \sum_{j=1}^{N} \beta_j T(t_i, s_j) + \beta_i \left\{ \sum_{\substack{j=1 \\ j\neq i}}^{N} A(t_i, s_j) - A(t_i, s_i) \right\} \\ &= \sum_{\substack{j=1 \\ j\neq i}}^{N} \beta_j T(t_i, s_j) + \beta_i \sum_{\substack{j=1 \\ j\neq i}}^{N} A(t_i, s_j), \quad t_i \in \Gamma. \end{aligned} \tag{16}$$

Then the diagonal elements of RMM in [11, 13] are given by

$$A(t_i, s_i) = \sum_{\substack{j=1 \\ j\neq i}}^{N} A(t_i, s_j), \quad i = 1, 2, \ldots, N. \tag{17}$$

Obviously, the bounded diagonal elements in Equation (17) are obtained based on the assumption that the source nodes are uniformly distributed. However, it's difficult to meet this condition for arbitrary shape domain problems.

A simple improvement of this problem can be obtained directly from Equations (13) and (14) as

$$A(t_i, s_i) = A^{(e)}(t_i, s_i) = \frac{1}{|l_i|} \sum_{\substack{j=1 \\ j\neq i}}^{N} A(t_i, s_j)|l_j|, \quad i = 1, 2, \ldots, N. \tag{18}$$

In [16], we have verified the validity of the diagonal elements in Equation (18). However, the curve lengths $\{|l_j|\}_{j=1}^{N}$ need to be computed by numerical integration, which increases the computational complexity and burden. Next, we will introduce a further improved desingularization technique without quadrature, while still keeps the solution accuracy and is valid for arbitrary shape domains.

To describe in a general sense, we suppose the boundary curve Γ is smooth, closed and can be represented as

$$x = p(\theta),\ y = q(\theta), \quad \theta \in [0, 2\pi], \tag{19}$$

where $p, q \in C^1[0, 2\pi]$. The case of piecewise smooth Γ can be treated similarly and is not discussed here. Based on Equation (19), the null-fields equation (12) can be rewritten as

$$\int_{\Gamma} A^{(e)}(t_i, s) d\Gamma(l) = \int_0^{2\pi} A^{(e)}(t(\theta_i), s(\theta)) \sqrt{p'(\theta)^2 + q'(\theta)^2} d\theta = \int_0^{2\pi} G_i(\theta) d\theta = 0, \tag{20}$$

where $G_i(\theta) = A^{(e)}(t(\theta_i), s(\theta)) \sqrt{p'(\theta)^2 + q'(\theta)^2}$.

DOI: 10.1002/jnm

Then Equation (20) is discretized by the composite trapezoidal integration rule [20], and we get

$$\begin{aligned}\int_0^{2\pi} G_i(\theta)d\theta &\approx \frac{1}{2}h\sum_{k=0}^{N-1}[G_i(\theta_k)+G_i(\theta_{k+1})]\\ &= \frac{1}{2}h[G_i(0)+2\sum_{k=1}^{N-1}G_i(\theta_k)+G_i(2\pi)]\\ &= h\sum_{k=1}^{N}G_i(\theta_k)\\ &= 0,\end{aligned} \tag{21}$$

where $h=\frac{2\pi}{N}$ and $\theta_k = kh,\ k=0,1,\ldots,N$. Here we suppose $G_i(0)=G_i(2\pi)$ since Γ is closed. It should be indicated that different h_j can also be employed in Equation (21), which ensures the meshfree property of the RMM.

Denote $g_i=\sqrt{p'(\theta_i)^2+q'(\theta_i)^2}$. Thus, from Equation (21) there is

$$A(t_i,s_i)=A^{(e)}(t_i,s_i)=-\frac{1}{g_i}\sum_{\substack{k\neq i\\ k=1}}^{N}A^{(e)}(t_i,s_k)g_k=\frac{1}{g_i}\sum_{\substack{k\neq i\\ k=1}}^{N}A(t_i,s_k)g_k, \tag{22}$$

where$(t_i,s_i)=(t(\theta_i),s(\theta_i))$. It is highlighted that our numerical results of RMM in the following sections are all computed with the diagonal elements in Equation (22). It has the same accuracy as the RMM with diagonal elements in Equation (18) but without the numerical integration.

3.2. The cutoff wavelength searching based on Chebfun

This section introduces the technique that extracts the minimum values that correspond to λ_c from Equation (9). A well-known theorem is

Theorem 3.1
Suppose function f is smooth on $[m,n]$ where its first and second order derivatives both exist. If there is $q\in(m,n)$ such that $f'(q)=0$ and $f''(q)>0$, then $(q,f(q))$ is a local minimum node of f on $[m,n]$.

However, as we indicated before, the two functions in Equations (8) and (9) are only piecewise smooth. They have some sharp nodes where their derivatives don't exit. Fortunately, Chebfun [17] has the ability to deal with such troublesome problem. It can detect the location of discontinuities and has a global rootfinding capability no matter the function is smooth or not. Thus, we can still use the rule provided in Theorem 3.1 to determine the λ_c. Actually, the function f will be approximated piecewisely by the Chebyshev polynomial in Chebfun. Then the derivatives of f can be computed accordingly. Since it has already been indicated precisely in literatures [17, 18, 19], we will not introduce more details about the principle used in Chebfun here. Our contribution is to use this powerful technique of Chebfun and to verify its ability to solve the cutoff wavelength problem. For convenience, we give the Matlab code of Chebfun in Figure 2, where the output parameter 'local_minima' contains the cutoff wavelength λ_c. We refer to this cutoff wavelength searching

Prepared using jnmauth.cls
DOI: 10.1002/jnm

```
% approximate f(lambda) by Chebyshev series on [m,n]
chebfun_f = chebfun(@(lambda) f(lambda), [m,n],
'splitting','on','vectorize');
% find extrema
r= roots(diff(chebfun_f));
% extract minima
local_minima = r(feval(diff(chebfun_f,2),r) > 0);
% plot solution
plot(chebfun_f); hold on
plot(local_minima,chebfun_f(local_minima),'or'); hold off
```

Figure 2. The Matlab code of Chebfun to search the cutoff wavelength.

method based on Chebfun as the CWcheb for short. For comparison, the conventionally used cutoff wavelength searching method based on figure plotting is called as the CWscan.

4. NUMERICAL EXPERIMENT

The proposed algorithm is tested with various numerical examples and compared with the MFS [7]. The analytical cutoff wavelength results in [1] are taken as reference solutions. All the calculations are dimensionless. In all examples, the semi-major axis of each elliptical waveguide is set as 1.0. And the figures of $f(\lambda)$ are all plotted under the 10 base logarithmic scale.

4.1. Comparison of the RMM and MFS with CWscan

As known, the CWscan method is reliable as long as the scanning step is small enough. Thus, we first verify the validity of the RMM combined with CWscan and compare it with the MFS. In Figure 3, the figures of $f(\lambda)$ defined in Equation (9) are plotted with $e = 0.5$ and 0.9 by the CWscan. Each local minimum corresponds to one cutoff wavelength. We can see the results of RMM agree well with the MFS results. Particularly, it can be observed the magnitude of $f(\lambda)$ for the RMM is much larger than that of the MFS. This is because the interpolation matrix A of the RMM is diagonally dominant and its determinant is almost equal to $\Pi_{j=1}^{N} A(j,j)$, which is numerically very large even if $\lambda = \lambda_c$. This phenomenon also shows the reasonability of using the local minimum finding instead of the root searching for the determinant function $f(\lambda)$.

We also study the influence of the source nodes location on the solution accuracy of the MFS. Figure 4 shows the MFS solutions of $e = 0.9$ with two different fictitious BCs. We can see the MFS gets exact solutions when $w = 1.3$ while gets totally distorted solutions when $w = 1.05$. Since it removes the need of fictitious sources boundary, the advantage of RMM is obvious.

4.2. Comparison of the RMM and MFS with CWcheb

As known, the CWscan is time-consuming. Thus, we will test the capability of the RMM and MFS combined with CWcheb. We take $e = 0.9$ for example and the results are shown in Figure 5. We can see the RMM results are accurate and stable when the nodes number changed from $N = 25$ to $N = 60$. It indicates the CWcheb is not sensitive for the RMM when the nodes number increased. However, the MFS results are only accurate when $N = 25$ and $w = 1.3$. The CWcheb fails for the

Prepared using jnmauth.cls
DOI: 10.1002/jnm

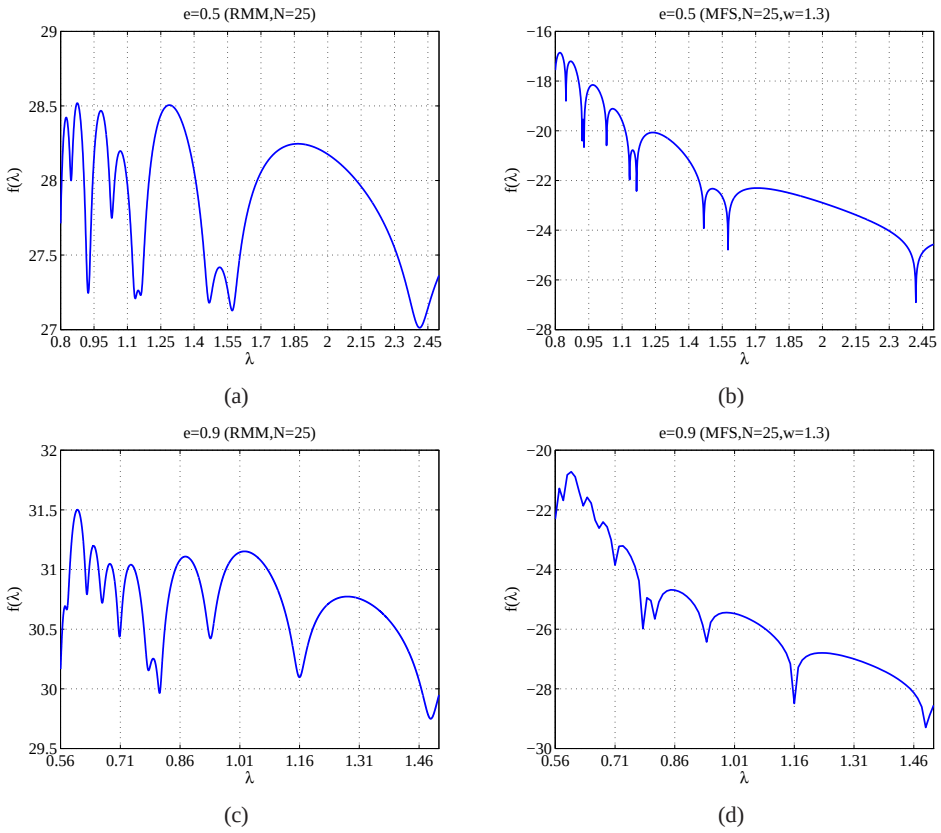

Figure 3. The $f(\lambda)$ curves of TM mode for $e = 0.5$ and 0.9.

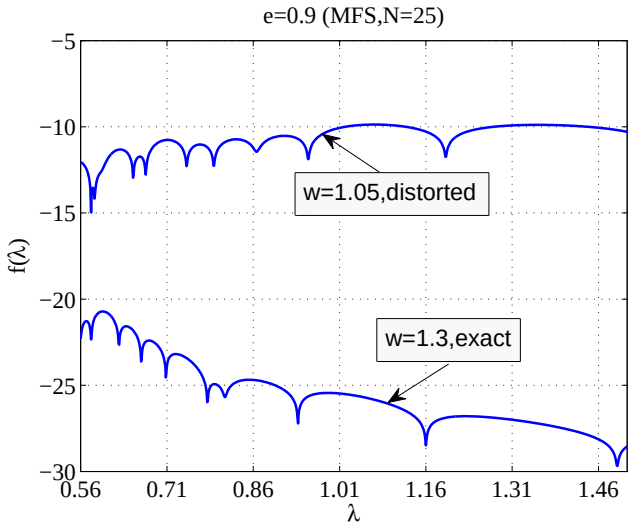

Figure 4. The $f(\lambda)$ curves by MFS with different fictitious source boundaries.

MFS when $N = 25, w = 1.4$ and $N = 40, w = 1.3$. It shows the change of source nodes number or fictitious boundary location of the MFS may distort the CWcheb results.

Prepared using jnmauth.cls
DOI: 10.1002/jnm

To analyze the reason behind this phenomenon, the condition numbers (CNs) of interpolation matrices of the RMM and MFS are plotted in Figure 5(f). We can see the CNs of the MFS are much higher than the RMM. And the CNs of the RMM are almost unchanged when N increases. From Figure 5, it can be observed the CWcheb only works when the CNs are low. This is because $f(\lambda)$ will vary very sharply when CN is large which makes the Chebyshev polynomial approximation to $f(\lambda)$ too hard. It results the obtained approximate Chebyshev curve incorrect and a lot of fictitious local minimum appear. Different from the MFS, whose interpolation matrices are usually ill-conditioned, which prevents the use of CWcheb, the RMM is well-conditioned and can work with the CWcheb smoothly. It shows the better compatibility of the RMM with the CWcheb than the MFS.

4.3. Comparison of the solution accuracy and computing time of the RMM and MFS

In this section, we check the accuracy of these two methods. The cutoff wavelengths of the first nine TM modes with $e = 0.5$ and $e = 0.9$ are shown in Tables I and II respectively. All these results of the two methods are obtained with CWcheb. And $w = 1.3$ is set for the MFS. We can see the MFS results are usually more accurate than the RMM. As seen in Table I, the 7th and 8th analytical cutoff wavelengths with $e = 0.5$ are very close. They are well distinguished in the MFS. But in the RMM, as limited by its solution accuracy, only single value 0.9241 (0.9246) lying inside these two exact ones is obtained when $N = 25$ ($N = 40$). However, when N increases to 60, the RMM also gets two accurate results for them.

In Figure 6, we plot the relative error curves for the cutoff wavelength of the dominate TM mode with different eccentricities. We find the solution accuracy of the RMM improves when N increases. The MFS obtains a better accuracy if e is smaller than 0.9. But opposite results are observed when e is close to 1. The solution accuracy of the MFS degenerates quickly when e is large. This is because the choose of fictitious boundary for the MFS is more challenging in such case. However, it's not a problem for the RMM.

The lower accuracy of the RMM compared to the MFS is due to the desingularization technique which employs the approximate discrete null fields equation. In contrast, the MFS takes the fictitious boundary instead and no approximation is brought in. However, the RMM solutions are also very satisfied compared to the analytical ones. Most importantly, the RMM is much stable than the MFS as mentioned before. It should also be noted that these CWcheb results in the two tables are completely consistent with the CWscan results under the step length 10^{-4}.

Table III shows the computing time for the results in Tables I and II by different methods on a Intel Core i7 950 CPU computer. It can be seen our new method (RMM combined with CWcheb) is much faster than the previous one (MFS combined with CWscan). The CWcheb reduces the computing time of the RMM obviously. The longest computing time belongs to the MFS combined with CWcheb. This is because the $f(\lambda)$ curve of the MFS is too sharp and it costs a lot of time to do the Chebyshev approximation in Chebfun. However, the CWcheb can solve all the cutoff wavelength together without worrying to lose solutions. Besides, we can also see the computing time of CWcheb increases slightly when the searching segment enlarged. This is another advantage of CWcheb over the CWscan.

DOI: 10.1002/jnm

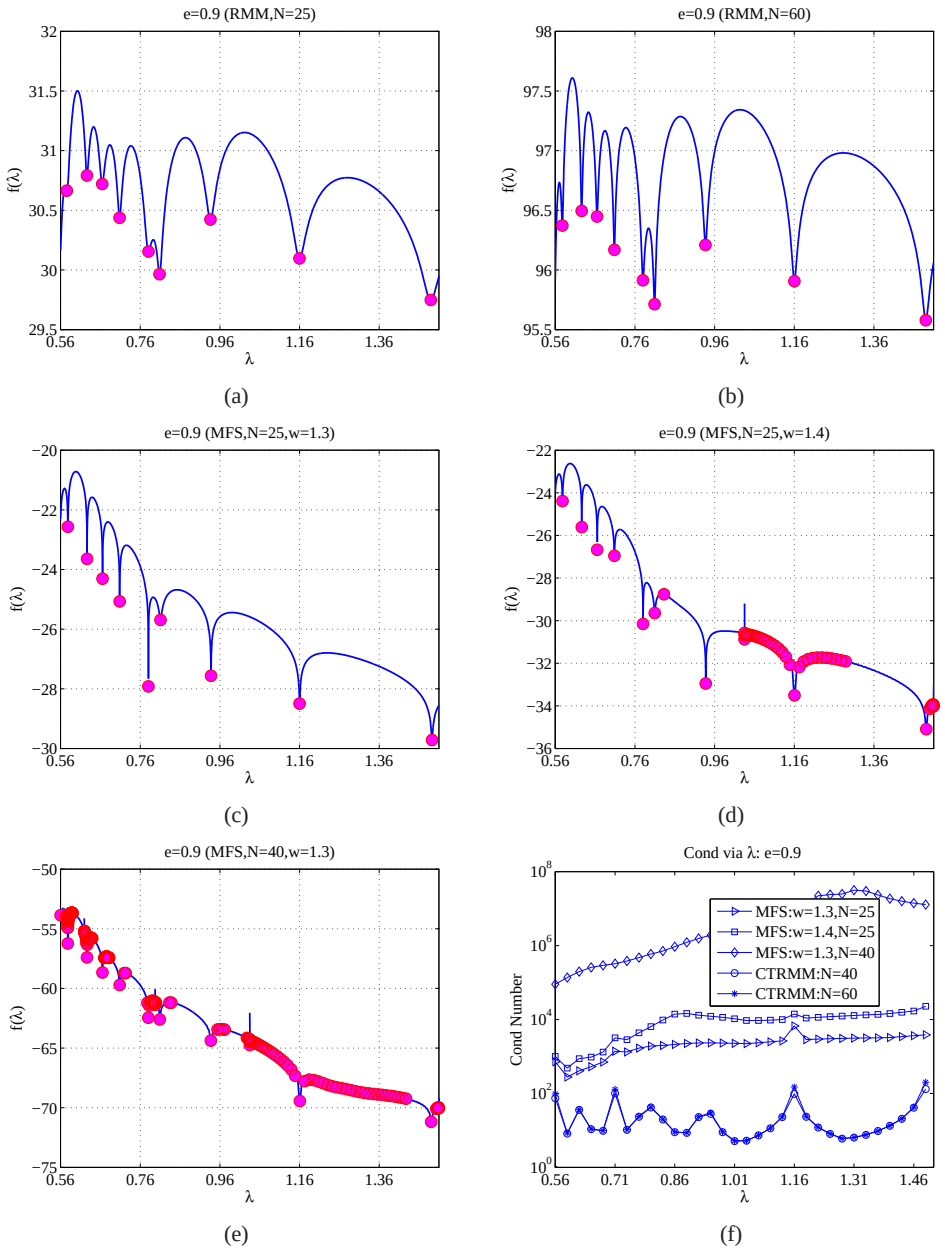

Figure 5. (a)-(e): the $f(\lambda)$ curves approximated by Chebfun; (f): the condition number curves of the MFS and RMM with $e = 0.9$.

5. CONCLUSION

This paper develops the RMM for solving the cutoff wavelength of elliptical waveguide and compares it with the MFS. We introduce an improved desingularization technique that makes the conventional RMM be applicable for arbitrary shape domain problems. Furthermore, instead of employing the commonly used scanning method, the novel local minimum finding technique based on Chebfun is combined with RMM for the first time to search the cutoff wavelength. It can reduce notably the computing time of the RMM and avoid to lose solutions. The numerical simulations

Prepared using jnmauth.cls
DOI: 10.1002/jnm

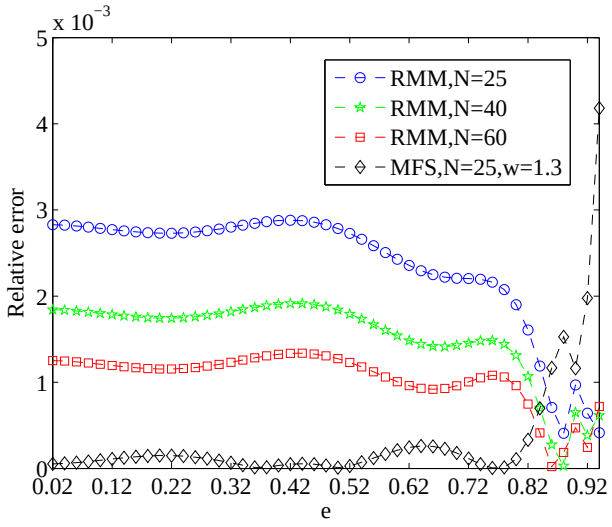

Figure 6. The relative error curves of dominant TM mode with different eccentricities.

show the RMM results are more stable than the MFS in two aspects. Namely, it avoids the fictitious boundary and has better compatibility with the CWcheb. The accuracy of the RMM is a little lower than the MFS but it's still satisfied. Our method provides another good candidate to solve the cutoff wavelength of elliptical waveguide. The property of the RMM allows it to be well applicable in other waveguides with different shapes.

ACKNOWLEDGEMENT

Part of this work was carried out at the department of Mathematics, Zhejiang University, China. And it was partially contained in the PhD thesis of Rencheng Song. This work was supported by the Singapore Temasek Defence Systems Institute under grant TDSI/10-005/1A.

REFERENCES

1. Zhang SJ, Shen YC. Eigenmode sequence for an elliptical waveguide with arbitrary ellipticity. *IEEE Transactions on Microwave Theory and Techniques* 1995;**43**:227–230.
2. Chu LJ, Electromagnetic waves in elliptic hollow pipes of metal. *Journal of Applied Physics* 1938: **9**: 583–591.
3. Mei ZL, Xu FY. A simple, fast and accurate method for calculating cutoff wavelengths for the dominant mode in elliptical waveguide. *Journal of Electromagnetic Waves and Applications* 2007;**21**:367–374.
4. Tsogkas GD, Roumeliotis JA, Savaidis SP. Cutoff wavelengths of elliptical metallic waveguides. *IEEE Transactions on Microwave Theory and Techniques* 2009;**57**:2406–2415.
5. Shu C. Analysis of elliptical waveguides by differential quadrature method. *IEEE Transactions on Microwave Theory and Techniques* 2000;**48**:319–322.
6. Jiang PL, Li SQ, Chan CH. Analysis of elliptical waveguides by a meshless collocation method with the wendland radial basis functions. *Microwave and Optical Technology Letters* 2002;**32**:162–165.
7. Young DL, Hu SP, Chen CW, Fan CM, Murugesan K. Analysis of elliptical waveguides by the method of fundamental solutions. *Microwave and Optical Technology Letters* 2005;**44**:552–558.
8. Fairweather G, Karageorghis A. The method of fundamental solutions for elliptic boundary value problems. *Advances in Computational Mathematics* 1998; **9**:69–95.
9. Chen JT, Chen PY. Null-field integral equations and their applications. In C. A. Brebbia, editor, *Boundary Elements and Other Mesh Reduction Methods XXIX*, pages 88–97. WIT Press, Southampton, 2007.

Prepared using jnmauth.cls
DOI: 10.1002/jnm

10. Young DL, Chen KH, Lee CW. Novel meshless method for solving the potential problems with arbitrary domain. *Journal of Computational Physics* 2005; **209**:290–321.
11. Chen KH, Kao JH, Chen JT, Young DL, Lu MC. Regularized meshless method for multiply-connected-domain Laplace problems. *Engineering Analysis with Boundary Elements* 2006;**30**: 882–896.
12. Chen KH, Chen JT, Kao JH. Regularized meshless method for antiplane shear problems with multiple inclusions. *International Journal for Numerical Methods in Engineering* 2008; **73**:1251–1273.
13. Young DL, Chen KH, Lee CW. Singular meshless method using double layer potentials for exterior acoustics. *Journal of the Acoustical Society of America* 2006; **119**:96–107.
14. Chen W, Lin J, Wang FZ. Regularized meshless method for nonhomogeneous problem. *Engineering Analysis with Boundary Elements* 2011; **35**:253–257.
15. Chen KH, Chen JT, Kao JH. Regularized meshless method for solving acoustic eigenproblem with multiply-connected domain. *CMES: Computer Modeling in Engineering and Science* 2006; **16**:27–40.
16. Song RC, Chen W. An investigation on the regularized meshless method for irregular domain problems. *CMES: Computer Modeling in Engineering and Science* 2009;**42**:59–70.
17. Pachón R, Platte RB, Trefethen LN. Piecewise-smooth chebfuns. *IMA Journal of Numerical Analysis* 2010; **30**:898–916.
18. Boyd JP. Computing zeros on a real interval through chebyshev expansion and polynomial rootfinding. *SIAM Journal on Numerical Analysis* 2002;**40**:1666–1682.
19. Battles Z, Trefethen LN. An extension of Matlab to continuous functions and operators. *SIAM Journal on Scientific Computing* 2004;**25**:1743–1770.
20. K. E. Atkinson. 1989. *An Introduction to Numerical Analysis* (2nd edn). John Wiley & Sons.

DOI: 10.1002/jnm

Table I. Cutoff wavelength of TM mode with $e = 0.5$

No.	Analytical Ref[1]	MFS	RMM		
		$N = 25$	$N = 25$	$N = 40$	$N = 60$
1	2.4196	2.4198	2.4130	2.4153	2.4167
2	1.5762	1.5762	1.5711	1.5736	1.5747
3	1.4673	1.4674	1.4679	1.4670	1.4669
4	1.1652	1.1652	1.1598	1.1630	1.1641
5	1.1336	1.1336	1.1355	1.1339	1.1336
6	1.0303	1.0303	1.0301	1.0301	1.0302
7	0.9289	0.9289	0.9241	0.9246	0.9275
8	0.9208	0.9208	\	\	0.9216
9	0.8478	0.8477	0.8472	0.8475	0.8476

Table II. Cutoff wavelength of TM mode with $e = 0.9$

No.	Analytical Ref[1]	MFS	RMM		
		$N = 25$	$N = 25$	$N = 40$	$N = 60$
1	1.4906	1.4925	1.4894	1.4898	1.4901
2	1.1607	1.1600	1.1598	1.1601	1.1603
3	0.9375	0.9377	0.9363	0.9368	0.9371
4	0.8093	0.8109	0.8085	0.8090	0.8091
5	0.7803	0.7804	0.7808	0.7802	0.7801
6	0.7083	0.7083	0.7081	0.7082	0.7082
7	0.6651	0.6653	0.6646	0.6647	0.6649
8	0.6262	0.6265	0.6262	0.6261	0.6261
9	0.5780	0.5783	0.5756	0.5771	0.5776

Table III. Computing time of different methods

e	Time(s)	CWcheb	CWscan
0.5	RMM	5.6	18.6
	MFS	21.8	17.1
0.9	RMM	5.9	10.3
	MFS	19.8	9.5

DOI: 10.1002/jnm